

A Chiral Paramagnetic Skymion-like Phase in MnSi

C. Pappas,¹ E. Lelièvre-Berna,² P. Falus,² P. M. Bentley,² E. Moskvin,^{1,3} S. Grigoriev,³ P. Fouquet,² and B. Farago²

¹*Helmholtz Center Berlin for Materials and Energy, Glienickerstr. 100, 14109 Berlin, Germany**

²*Institut Laue-Langevin, 6 rue Jules Horowitz, 38042 Grenoble, France*

³*Petersburg Nuclear Physics Institute, 188300 Gatchina, Leningrad District, Russia*

(Dated: May 8, 2022)

We present a comprehensive study of chiral fluctuations in the reference helimagnet MnSi by polarized neutron scattering and Neutron Spin Echo spectroscopy, which reveals the existence of a completely left-handed and dynamically disordered phase. This phase may be identified as a spontaneous skymion phase: it appears in a limited temperature range just above the helical transition T_C and coexists with the helical phase at T_C .

Chirality is ubiquitous in nature and of fundamental importance both on the microscopic level and in our everyday life. The break of symmetry between right and left manifests itself in parity violation, governs biological structures such as DNA and can also be experienced in the organisation of our own body. In magnetism, chirality is evident in solitons [1], systems with geometric frustration [2] and metallic systems with non-centro-symmetric lattice structures, where the resulting anti-symmetric Dzyaloshinski-Moriya (DM) interactions [3, 4] introduce a parity breaking term in the Hamiltonian [5]. The DM term has the form $\vec{M} \times (\vec{\nabla} \times \vec{M})$ and is more than a perturbation giving rise to the peculiar canted magnetic arrangements found in high temperature superconductors [6] or the cycloid spin structures in multiferroics [7, 8]. In the non-centrosymmetric weak itinerant-electron ferromagnet MnSi, DM induced chirality comes in close interplay with Fermi liquid behavior and quantum fluctuations [9]. The Hamiltonian of MnSi comprises three hierarchically ordered magnetic interaction terms with well separated energy scales [10], which allow to distinguish between different contributions. The strongest ferromagnetic exchange interaction aligns the spins, the weaker chiral Dzyaloshinski-Moriya (DM) term twists them into a helix and the weakest Anisotropic Exchange (AE) or crystal field term pins the helix propagation vector $\vec{\tau}$ along the $\langle 111 \rangle$ crystallographic directions. The helical order appears below $T_C \approx 29$ K. It is a left-handed helix with a period of $\ell \sim 175$ Å ($\tau \approx 0.036$ Å⁻¹) and all magnetic moments perpendicular to the helix vector [11].

In this letter we concentrate on the chiral correlated paramagnetic or spin liquid phase of MnSi just above T_C , where intense diffuse neutron scattering spreads homogeneously over the surface of a sphere with radius τ . This unusual feature emerges as a ring on the two-dimensional small angle neutron scattering patterns and the rings reduce to half-moons if the beam is polarized. This is illustrated by figure 1, which reproduces spectra from [12]. Numerous theoretical studies were devoted to explain this phase invoking possibilities such as unpinned helical order [12, 13] or condensation of chiral order pa-

rameters [14]. Recent Monte Carlo simulations assuming the hierarchical hamiltonian of MnSi show that the helical phase is preceded by a disordered skymion phase similar to the partial order in liquid crystals [15], which sets in at $T_C \approx T_C + 1$ K (see supplementary information of [15]). Skymions are non-linear solutions introduced in the early '60s by Skyrme [16] to bridge the gap between waves and particles in the wave-particle duality concept. In MnSi a Skymion lattice was recently identified under magnetic field [17]. At zero magnetic field skymions would result from the inherent topological vortex-like singularities of the isotropically twisted spin liquid phase (see insert on Figure 2b).

Spin correlations and fluctuations of MnSi have been extensively studied by triple axis spectroscopy (TAS) at Brookhaven in the mid-80s [18] and more recently with polarized neutrons [19]. These studies, however, did not have the resolution needed to see fluctuations close to the helical transition. We opted for neutron spin echo spectroscopy (NSE) [20], which reaches the highest energy resolution (<1 neV) among all neutron scattering techniques. We also combined NSE with spherical neutron polarimetry (SNP) [21] to the polarimetric NSE technique [22] for a rigorous analysis of chiral fluctuations.

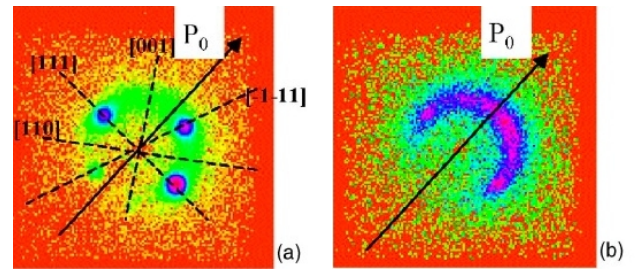


FIG. 1: Polarized neutron small angle scattering patterns measured by [12] below (a) and (b) slightly above the helimagnetic transition of MnSi. The P_0 vectors mark the polarization vector of the incoming neutron beam.

The starting point of our study is the formalism developed almost simultaneously by Blume [23] and Maleyev

[24] in the early '60s. The magnetic scattering cross-section for thermal neutrons may be written as:

$$\sigma = \vec{M}_\perp \cdot \vec{M}_\perp^* + \vec{P}' \cdot \Im(\vec{M}_\perp \times \vec{M}_\perp^*) \quad (1)$$

where \vec{P}' is the polarization vector of the incident beam and the magnetic interaction vector \vec{M}_\perp is the projection of the magnetic structure factor onto a plane perpendicular to the scattering vector \vec{Q} . The (imaginary) vector product is the chiral term characteristic of the spiral structure.

In MnSi the helix is described by two orthogonal vectors \vec{M}_y and \vec{M}_z of the same amplitude, which are perpendicular to the helix vector $\vec{\tau}$. At the helical Bragg peaks $\vec{\tau}_{111}$ the sample orientation is such that $\vec{Q} \parallel \vec{\tau}$ and for a left handed helix $\vec{M}_\perp = \vec{M}_y \cos(\vec{q} \cdot \vec{r}) - \vec{M}_z \sin(\vec{q} \cdot \vec{r})$. The cross-section is therefore maximum for $\vec{P}' = \hat{Q}$ and completely extinct for $\vec{P}' = -\hat{Q}$. As already pointed out in [12], this extinction is responsible for the characteristic half-moon small angle scattering patterns seen with polarized neutrons above T_C . It gives a very precise determination of the weight of the dominant chiral domain $\eta = |\vec{M}_\perp \times \vec{M}_\perp^*| / (\vec{M}_\perp \cdot \vec{M}_\perp^*)$. η can also be determined from the polarization vector of the scattered neutron beam \vec{P} :

$$\begin{aligned} \vec{P}\sigma &= -\vec{P}'(\vec{M}_\perp \cdot \vec{M}_\perp^*) + 2\Re((\vec{P}' \cdot \vec{M}_\perp^*)\vec{M}_\perp) \dots \\ &\dots -\Im(\vec{M}_\perp \times \vec{M}_\perp^*) \end{aligned} \quad (2)$$

The first two terms lead to the conventional π rotation of the polarization vector around \vec{M}_\perp . The chiral term creates a polarization (anti)parallel to \hat{Q} independently from the incoming beam polarization. Complete knowledge of Eq. 2 implies complete knowledge and control of \vec{P}' and \vec{P} independently from each other. This is achieved with spherical neutron polarimetry using Cryopad, which brings \vec{P}' and \vec{P} either along $\hat{x} = \hat{Q}$, \hat{z} (perpendicular to the scattering plane) or \hat{y} , which completes the right-handed cartesian set [25]. This procedure determines the polarization matrix:

$$\mathbb{P}_{\alpha,\beta} = \frac{P_{\alpha,\beta}}{|\vec{P}'|} = \frac{\tilde{P}_{\alpha,\beta} P'_\alpha + P_\beta^\dagger}{|\vec{P}'|} \text{ with } (\alpha,\beta) \in \{x,y,z\} \quad (3)$$

where \tilde{P} is the polarization tensor of the non-chiral terms and P^\dagger the polarization created by the chiral term. At $\vec{\tau}_{111}$, $\hat{x} \parallel \vec{\tau}$ and only the first row of the matrix is non-zero. The ideal matrix is given in Table I, where ζ determines the chirality of the helix: $\zeta = +1$ for right and $\zeta = -1$ for left handed chirality. η measures the fraction of the dominant chiral domain. $\eta = 1$ for a single domain and $\eta = 0$ for a disordered state or equally populated chiral domains.

The polarimetric measurements were done with Cryopad on the NSE spectrometer IN15 of the ILL. With the polarimetric NSE configuration it was possible to

TABLE I: Ideal and measured polarization matrix $\mathbb{P}_{\alpha,\beta}$ at $\vec{\tau}_{111}$. For details see text.

$\beta \setminus \alpha$	ideal			25K		
	x	y	z	x	y	z
x	-1	$\eta\zeta$	$\eta\zeta$	-0.99(1)	-0.99(1)	-0.99(1)
y	0	0	0	0.05(2)	0.05(2)	0.05(2)
z	0	0	0	-0.01(2)	-0.01(2)	-0.01(2)

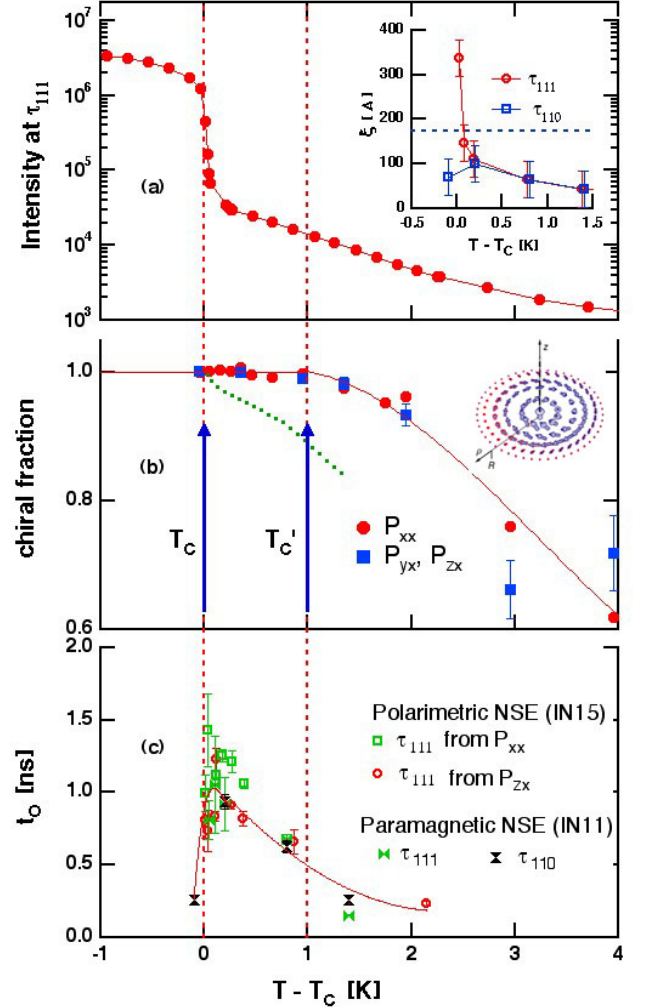


FIG. 2: Intensity at the position of the $\vec{\tau}_{111}$ helical peak (a), chiral fraction of the dominant left handed domain (b) and characteristic time t_0 of the fluctuations at $\vec{\tau}_{111}$ and $\vec{\tau}_{110}$ (c). In (b) the red circles are deduced from the extinction ($\mathbb{P}_{x,x}$ eq. 1), the blue squares from the non-diagonal terms $\mathbb{P}_{y,x}$ and $\mathbb{P}_{z,x}$ and the green dotted line is calculated from ξ_{111} and eq. 4. The error bars are calculated from the counting rates and do not include systematic errors. For the sake of comparison between different cryogenic setups the data are plotted against $T - T_C$. The lines are guides for the eyes.

determine the matrix $\mathbb{P}_{\alpha,\beta}$ and at the same time ac-

cess the intermediate scattering function $I(Q,t)$ of each non-zero term. These measurements were complemented by “conventional” NSE measurements on IN11 (ILL). The measurements were done at $\lambda=9$ Å (IN15) and 5.5 Å (IN11) with $\Delta\lambda/\lambda=15\%$ FWHM and a Q -resolution of ~ 0.005 Å $^{-1}$ FWHM. Most of the measurements were carried out at $\vec{\tau}_{111}$. Additional spectra were recorded on IN11 around $\vec{\tau}_{110}$ (see figure 1). It was also possible to extract precise information on the $q = Q - \tau$ dependence of the relaxation by analyzing slices of the detector at constant distance from the 000 point. The MnSi single crystal was the same as in previous experiments [12] with the B20 lattice structure ($P2_13$) and a lattice constant of 4.558 Å.

The transition temperature $T_C = 29.05 \pm 0.05$ K is defined from the sudden increase by more than one order of magnitude of the neutron intensity at $\vec{\tau}_{111}$ (figure 2a), which confirms the weak first order transition with strong second-order features seen on specific heat [26].

The Ornstein-Zernike analysis of the q dependence of the intensity around $\vec{\tau}_{111}$ and $\vec{\tau}_{110}$ leads to the correlation lengths ξ_{111} and ξ_{110} , shown on the insert of figure 2a. They quantify the extent of correlations along the helix vector $\vec{\tau}$ and are very close to previous results [12]. ξ_{110} stays significantly smaller than the pitch of the helix and shows a maximum slightly above T_C , whereas ξ_{111} diverges and reaches the pitch of the helix (dashed line) at $\sim T_C+0.05$ K, probably triggering the first order transition.

The polarization matrix was measured with an incident beam polarization of 97% and the data were corrected for the background signal. At $\vec{\tau}_{111}$ the calculated and measured matrices of the helical phase at 25 K are in excellent agreement with each other (Table I) confirming the stabilisation of a single-domain left-handed helix with $\eta = 1, \zeta = -1$. When increasing the temperature, the polarization matrix $\mathbb{P}_{\alpha,\beta}$ is unaffected by the first order transition and remains unchanged up to $T_{C'} \approx T_C + 1$ K. Also the extinction of the scattering when $\vec{P}' = -\hat{\tau}$ (eq. 1) is complete up to $T_{C'}$. All values of η , plotted in figure 2b, reveal the existence of a new phase between T_C and $T_{C'}$. This is a completely single domain even though the correlations are significantly shorter than ℓ : at $T_{C'}$ the mean correlation length ξ does not exceed $\sim \ell/4$. This result contrasts with the common experimental [27] and theoretical [12] picture based on the hierarchy of the interactions, according to which MnSi behaves as a ferromagnet at distances shorter than ℓ and for $\xi < \ell$. In fact our experimental results show a more complex situation and the slow decrease of the chiral fraction η displayed in figure 2c spreads over a very wide temperature range. Even at 50 K (T_C+20 K) where correlations do not exceed 7 Å [18], we found $\eta \sim 0.203 \pm 0.024$.

A mean field description of paramagnetic fluctuations in a ferromagnet in the presence of DM interactions was given in [12] and renders the main features of MnSi: ex-

tinction of the scattering at $\vec{P}' = -\hat{\tau}$ or intensity maximum at the sphere $Q = \tau$ (figure 1). The theory also gives a simple relation between η and the correlation length ξ :

$$\eta = 2Q\tau / (Q^2 + \tau^2 + 1/\xi^2) \quad (4)$$

From the measured ξ_{111} values we calculated the dotted green line on figure 2b, which however does not reproduce the experimental findings. This strong discrepancy underlines the non-trivial character of the spin liquid phase of MnSi, in particular of the phase between T_C and $T_{C'}$.

In the following we will discuss the results of our NSE measurements. NSE spectroscopy gives the normalized intermediate scattering function $I(Q,t) = S(Q,t)/S(Q,0)$, which is the time-energy Fourier transform of the scattering function $S(Q,\omega)$. The fluctuations of the single domain chiral spin liquid phase were measured with standard NSE. The fluctuations for $\vec{P}' \perp \tau_{111}$ ($\mathbb{P}_{z,x}$ or $\mathbb{P}_{y,x}$) and $\vec{P}' \parallel \tau_{111}$ ($\mathbb{P}_{x,x}$) at the $\vec{\tau}_{111}$ position were measured with polarimetric NSE. Figure 3 shows the intermediate scattering function for the non-diagonal term $\mathbb{P}_{z,x}$. We find exponential relaxations superimposed on an elastic contribution due to the Bragg peak, which were fitted by the function $I(Q,t) = a \exp(-t/t_0) + (1-a)$. The elastic fraction $(1-a)$ evolves from $\sim 20\%$ to 100% within 0.2 K following the fast increase of the intensity in figure 2a. The onset of the Bragg peak masks the decay of $I(Q,t)$ at T_C . On the other hand, at $\vec{\tau}_{110}$ there are no Bragg peaks and fluctuations may be seen also below T_C . The measurements were extended up to $T_C + 2$ K, where they agree with the previous TAS [18, 19] and preliminary resonance NSE results [28].

All values of t_0 are plotted against temperature in figure 2c. The existence of finite relaxation times at these temperatures rules out the interpretation in terms of quasi-static correlations suggested by [9]. The measured relaxation times are rather typical for correlated systems such as magnetic nanoparticles [29] or ferromagnets at

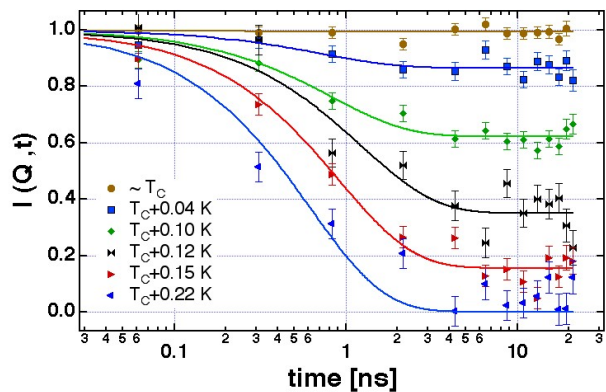


FIG. 3: Dynamic correlations at the position of one of the helical Bragg peaks $\vec{\tau}_{111}$ measured by polarimetric NSE for the $\mathbb{P}_{z,x}$ term of the polarization matrix (Table I).

T_C [30]. All t_0 (at $\bar{\tau}_{111}$ and $\bar{\tau}_{110}$) fall on top of each other within experimental error bars: the direction of the incident polarization vector or the particular position on the sphere with radius τ have no effect on the observed dynamics. The fluctuations are governed by the correlation length at τ_{110} without any sign of slowing down at τ_{111} , i.e. at the position where the Bragg peak appears. Consequently, the fluctuating chiral spin liquid phase does not develop to the helical phase. The two phases coexist close to T_C and ξ_{111} may be decomposed as: $\xi_{111} = \alpha \xi_{fluct} + (1 - \alpha) \xi_{static}$ with $\xi_{fluct} = \xi_{110}$ reflecting the fluctuating spin liquid fraction α and ξ_{static} the static component of the helical phase. It has been suggested that fluctuations may drive the transition in MnSi to first order [10, 31, 32]. Our present high resolution data rule out any interplay between fluctuations and the first order helical transition.

Dynamic scaling relates the characteristic relaxation time to the correlation length: $t_0 \propto \xi^z$, with z the dynamic exponent. Below $T_{C'}$ we found $t_0 \propto \xi_{fluct}$ leading to $z \approx 1$, an unconventional value much lower than in 3D ferromagnets ($z=5/2$) or antiferromagnets ($z=3/2$). Such a low value could reflect a locally reduced dimensionality with the spins pinned at the local helical planes.

Above T_C the Bragg peaks disappear and the correlation length becomes considerably shorter than the pitch of the helix. In spite of that all spins remain pinned into the local helical plane up to $T_{C'}$. This is exactly the theoretically predicted temperature of formation of a skyrmionic ground state in MnSi [15]. It is also the temperature range of a broad maximum in the specific heat [26]. Skyrmions would account for the inherent topological singularities of this single domain spin liquid phase, which gives a scattering with rotational symmetry. Skyrmionic textures are energetically favourable at short distances, which would favor structures with the magnetic moments decreasing with increasing distance from the vortex center [15]. In the spin liquid phase the mean magnetic moment decreases continuously with increasing distance d following the typical correlation function $\sim \exp(-d/\xi)/d$. The correlation length $\xi_{fluct} = \xi_{110}$ would, therefore, give a natural measurement of the skyrmion radius, which would not exceed $\ell/2$ at T_C stabilizing the single domain spin liquid phase. That skyrmionic solutions are energetically more favourable at short lengths would explain the slow decrease of η above T_C and its finite value even at $T_C+20\text{K}$ (50 K).

In summary, these first polarimetric NSE measurements provide the missing link in getting a consistent picture of the spin liquid phase of MnSi above T_C . High resolution neutron spin echo spectroscopy and polarimetry evidence the existence of a disordered skyrmion phase, a

completely chiral single domain and strongly fluctuating new state of matter in a very narrow temperature range of ~ 1 K above the helical phase of MnSi.

C.P. thanks P. Böni and E.L.-B. thanks P.J. Brown for fruitful discussions. The authors acknowledge the support of the ILL technical teams in particular E. Bourgeat-Lami, C. Gomez and E. Thaveron. Special thanks go to Thomas Krist for the compact solid state polarizer, which enabled the polarimetric NSE measurements. This project was partly supported by the European Commission under the 6th Framework Programme through the Key Action: Strengthening the European Research Area, Research Infrastructures. Contract no: RII3-CT-2003-505925."

* Electronic address: pappas@helmholtz-berlin.de

- [1] H. B. Braun et al., *Nature Physics* **1**, 159 (2005).
- [2] V. P. Plakhty et al., *Phys. Rev. Lett.* **85**, 3942 (2000).
- [3] I. E. Dzyaloshinski, *J. Phys. Chem. Solids* **4**, 241 (1958).
- [4] T. Moriya, *Phys. Rev.* **120**, 91 (1960).
- [5] S. V. Maleyev, *Phys. Rev. B* **73**, 174402 (2006).
- [6] M. B. Silva Neto and L. Benfatto, *Phys. Rev. B* **75**, 140501(R) (2007).
- [7] T. Goto et al., *Phys. Rev. Lett.* **92**, 257201 (2004).
- [8] T. Lottemoser et al., *Nature* **430**, 541 (2004).
- [9] C. Pfleiderer et al., *Nature* **427**, 227 (2004).
- [10] P. Bak and M. H. Jensen, *J. Phys. C* **13**, L881 (1980).
- [11] G. Shirane et al., *Phys. Rev. B* **28**, 6251 (1983).
- [12] S. V. Grigoriev et al., *Phys. Rev. B* **72**, 134420 (2005).
- [13] J. M. Hopkinson and H.-Y. Kee, *Phys. Rev. B* **79**, 014421 (2009).
- [14] S. Tewari et al., *Phys. Rev. Lett.* **96**, 047207 (2006).
- [15] U. K. Röbller et al., *Nature* **442**, 797 (2006).
- [16] T. Skyrme, *Proc. R. Soc. Lond. Ser. A* **260**, 127 (1961).
- [17] S. Mühlbauer et al., *Science* **323**, 915 (2009).
- [18] Y. Ishikawa et al., *Phys. Rev. B* **31**, 5884 (1985).
- [19] B. Roessli et al., *Phys. Rev. Lett.* **88**, 237204 (2002).
- [20] F. Mezei, *Neutron Spin Echo*, vol. 128 of *Lecture Notes in Physics* (Springer Verlag, Berlin, 1980).
- [21] F. Tasset, *Physica B* **156-159**, 627 (1989).
- [22] C. Pappas et al., *Nucl. Inst. and Methods in Phys. Res. A* **592**, 420 (2008).
- [23] M. Blume, *Phys. Rev.* **130**, 1670 (1963).
- [24] S. Maleyev et al., *Fiz. Tv. Tela* **4**, 3461 (1962).
- [25] P. J. Brown, *Physica B* **297**, 198 (2001).
- [26] S. M. Stishov et al., *Phys. Rev. B* **76**, 052405 (2007).
- [27] C. Pfleiderer et al., *Phys. Rev. B* **55**, 8330 (1997).
- [28] P. Böni et al., *E21 Annual report* (TU München, 2006).
- [29] H. Casalta et al., *Phys. Rev. Lett.* **82**, 1301 (1999).
- [30] F. Mezei, *Phys. Rev. Lett.* **49**, 1096 (1982).
- [31] S. A. Brazovskii et al., *Sov. Phys. JETP* **43**, 1178 (1976).
- [32] D. Belitz and T. R. Kirkpatrick, *Nature Physics* **3**, 15 (2007).